SARS-CoV-2 infected host cell proteomics reveal potential therapy targets

CURRENT STATUS: UNDER REVIEW

nature research

Denisa Bojkova
Institute of Medical Virology, University Hospital Frankfurt

Kevin Klann
Institute of Biochemistry II, Faculty of Medicine, Goethe University

Benjamin Koch
Medical Clinic III, Nephrology, University Hospital Frankfurt

Marek Widera
Institute of Medical Virology, University Hospital Frankfurt

David Krause
Institute of Biochemistry II, Faculty of Medicine, Goethe University

Sandra Ciesek
Institute of Medical Virology, University Hospital Frankfurt

Jindrich Cinatl
Institute of Medical Virology, University Hospital Frankfurt

cinatl@em.uni-frankfurt.de*Corresponding Author*

Christian Münch
Institute of Biochemistry II, Faculty of Medicine, Goethe University; Frankfurt Cancer Institute; Cardio-Pulmonary Institute

ch.muench@em.uni-frankfurt.de*Corresponding Author*

DOI:
10.21203/rs.3.rs-17218/v1

SUBJECT AREAS
General Cell Biology & Physiology *Virology*

KEYWORDS
SARS-CoV-2, cellular infection profile, translatome and proteome proteomics

Abstract

A novel coronavirus was recently discovered and termed SARS-CoV-2. Human infection can cause coronavirus disease 2019 (COVID-19), for which, at this point, over 80,000 cases resulting in over 2,500 deaths have been reported in over 40 countries. SARS-CoV-2 shows some similarities to other coronaviruses. However, treatment options and a cellular understanding of SARS-CoV-2 infection are lacking. Here we identify the host cell pathways modulated by SARS-CoV-19 infection and reveal that drugs targeting pathways prevent viral replication in human cells. We established a human cell culture model for infection with SARS-CoV-2 clinical isolate. Employing this system, we determined the SARS-CoV-2 infection profile by translatome and proteome proteomics at different times after infection.

These analyses revealed that SARS-CoV-2 reshapes central cellular pathways, such as translation, splicing, carbon metabolism and nucleic acid metabolism. Small molecule inhibitors targeting these pathways were tested in cellular infection assays and prevented viral replication. Our results reveal the cellular infection profile of SARS-CoV-2 and led to the identification of drugs inhibiting viral replication. We anticipate our results to guide efforts to develop therapy options for COVID-19.

Authors Denisa Bojkova, Kevin Klann, and Benjamin Koch contributed equally to this work

Data associated with the preprint has been made available on the authors' website

Introduction

At the end of the year 2019, a cluster of severe pneumonia of unknown cause was described in Wuhan (Eastern China) and strikingly a SARS-like acute respiratory distress syndrome (ARDS) noted in many patients. Early in January 2020, next and third generation sequencing revealed a novel coronavirus (originally termed 2019-nCoV, now SARS-CoV–2)

as the causal factor for the disease later designated COVID–191. It has currently spread to every Chinese province and, via global hubs, to many international countries and federations2. Clinical symptoms in severe disease center on fever, dry cough and fatigue. Also muscle pain, headache or confusion, abdominal pain, nausea, vomiting and diarrhoea have been observed3–6. For severe cases, laboratory results have shown lymphopenia, hypercytokinemia, disseminated intravasal coagulation and acute kidney injury. Patients who develop ARDS can deteriorate in a short period of time and die of multiple organ failure3–6. SARS-CoV–2 shows high infectivity resulting in rapid spreading7,8. The overall mortality rate for hospitalized patients is reported to be between 2.3%9 and 11% 5. Currently, there is no established therapy for COVID–19. Treatment is mainly based on supportive and symptomatic care, i.e. treating complications such as organ failure and secondary infections4,9,10. Therefore, the development of therapies inhibiting SARS-CoV–2 infection or replication are urgently needed. Using the protection of SARS-CoV–2 survivors (i.e. plasma from recovered COVID–19 patients) could be one option, but is not easily applicable for the great number of affected patients. Another approach is repurposing drugs that have been used for other indications, identified by high-throughput screening of drug libraries. This resulted in the identification of a number of clinically approved drugs that inhibited replication of highly pathogenic coronaviruses, such as MERS-CoV or SARS-CoV, in experimental models11. In order to fasten this approach and to take into consideration the particular biology of the virus of interest, molecular examination of infected cells by unbiased proteomics approaches offers a potent strategy for the identification of pathways relevant for viral pathogenicity as well as potential drug targets. This strategy depends on the availability of cell culture models permissive for virus infection and sensitive proteomics approaches for temporal infection profiling in cells. We recently succeeded to isolate SARS-CoV–2 from samples of travellers returning

from Wuhan (China) to Frankfurt (Germany) by using the human colon epithelial carcinoma cell line Caco–212. In addition, we lately described a novel method—multiplexed enhanced protein dynamics (mePROD) proteomics—enabling the determination of translatome and proteome changes at high temporal resolution, using a combination of metabolic labelling of newly synthesized proteins and tandem mass tags13.

Due to determination of translation changes by naturally occurring heavy isotope SILAC labelling, this method does not affect cellular behaviour and therefore allows a perturbation- free and unbiased analysis of the cellular response to viral infection.

In this study, we used quantitative translatome and proteome mass spectrometry to profile the cellular response to SARS-CoV–2 infection in permissive human Caco–2 cells. We monitored different time points post infection and identified key determinants of the host cell response to infection. These findings revealed potential pathways as drug targets for SARS-CoV–2 infection. We tested several such drugs targeting translation, proteostasis, glycolysis, splicing and nucleotide synthesis. These drugs inhibited SARS-CoV–2 replication at non-toxic concentrations, indicating therapeutic strategies for COVID–19.

Results

SARS-CoV–2 rapidly replicates in Caco–2 cells

To investigate potential antiviral compounds against SARS-CoV–2, we established a highly permissive SARS-CoV–2 cell culture model, characterized by fast progression of viral infection with visible cytopathogenic effect (CPE) already after 24 hours (Fig. 1a). To determine if productive viral infection takes place in this model, we measured viral RNA copies in supernatant during a 24 hour time period (Fig. 1b). The number of SARS-CoV–2 RNA molecules increased continuously after infection (Fig. 1c), indicating that the virus

undergoes full replicatory cycles in our cell culture model. Taken together, we established a functional SARS-CoV–2 cell culture model that allows investigation of the different steps of the SARS-CoV–2 life cycle in cells.

Translation inhibitors prevent SARS-CoV–2 replication

To determine the temporal profile of SARS-CoV–2 infection, we infected Caco–2 cells with SARS-CoV–2 at a multiplicity of infection of one, cultured them for a range of 2–24 hours and quantified translatome and proteome changes by mePROD proteomics compared to mock- infected samples (Fig. 2a, Supplementary Table 1). In each of three replicates, we quantified relative translation rates and relative protein levels for approximately 4,200 proteins and over 7,000 proteins, respectively. Dimension reduction by principal component analysis (PCA) showed that replicates clustered closely and revealed a first separation of infected samples from mock controls after 6 hours of infection (Fig. 2b). The translational landscape consecutively reshaped with longer infection times. Many RNA viruses decrease cellular protein synthesis, as has been suggested for SARS-CoV–114,15. However, when monitoring global translation rates, only minor changes were observed with a maximum of a 23% decrease in translation after 10 hours of infection with SARS-CoV–2 (Fig. 2c and Extended Data Fig. 1). To examine the kinetics of viral protein expression, we quantified the translation of viral proteins across time points (Fig. 2d). As expected, viral protein synthesis increased over time, starting 6 hours after transfection. Viral protein translation continuously accelerated, suggesting an increase in either translation efficiency or mRNA levels of viral genes. To identify pathways potentially important for virus amplification in cells, we determine host proteins that correlated with translation kinetics of viral proteins. Standardized (Z score), averaged profiles of all quantified viral proteins were used as reference profiles, distance to this profile calculated for all quantified host proteins, and a network analysis carried out for the top 10%

quantile of nearest profiles (Extended Data Fig. 1b). Pathway analyses of the network revealed extensive remodelling of translational patterns of the host translation machinery itself, potentially explaining how a significant change in global protein synthesis is avoided (Fig. 2c, e, Extended data Fig. 1c). In addition, we detected significant enrichment of components of several other pathways, such as antigen presentation or vesicular trafficking.

Host translation has been targeted previously11,16 to inhibit replication of diverse coronaviruses such as SARS-CoV–1 or MERS-CoV with FDA approved small molecules (Extended Data Fig. 1d). In contrast to other viruses, for which host protein synthesis has been reported to be repressed to allow increased synthesis of viral proteins14,15, our data suggested that SARS-CoV–2 only caused minor changes in host translation capacity (Fig. 2c). Thus, we speculated that SARS-CoV–2 replication might be more sensitive to translation inhibition, since viral proteins compete with host proteins for efficient translation. We tested two translation inhibitors—cycloheximide (inhibitor of translation elongation) and emetine (inhibits 40S ribosomal protein S14)—for their ability to reduce SARS-CoV–2 replication.

Antiviral activity of these translation inhibitors against different coronaviruses had been observed previously (Extended Data Fig. 1d)11,16. All compounds caused significant inhibition of SARS-CoV–2 replication at non-toxic concentrations (Fig. 2f, g and Extended Data Fig. 1e, f). Taken together, analysing the translatome of cells infected with SARS-CoV–2 revealed the temporal profile of viral and host protein responses leading to the discovery of translation inhibitors as potent inhibitors of SARS-CoV–2 replication in cells.

Regulation of cellular pathways by SARS-CoV–2 infection

Next, we characterized changes in cellular protein networks upon SARS-CoV–2 infection at the level of total protein abundance. To obtain a general understanding of host proteome

changes after infection, we analysed system-wide changes in protein levels over time (Fig. 3a, Supplementary Table 2). While only minor host proteome changes were observed at early infection time points, the proteome underwent extensive modulation 24 hours post infection. Hierarchical clustering identified two main clusters of proteins regulated: The first cluster consisted of proteins reduced during infection and mainly included proteins belonging to cholesterol metabolism (Extended Data Fig. 2 and Supplementary Table 3). The second cluster was composed of proteins increased by infection and revealed strong increases in RNA modifiers, such as spliceosome components, and carbon metabolism (Fig. 3b, c, Extended data Fig. 3a and Supplementary Table 4). Remarkably, for most spliceosome components increased by SARS-CoV–2, direct binding to viral proteins of SARS-CoV–1 or other coronaviruses has been shown (Extended data Fig. 3b)9,17–21. Thus, we tested whether inhibition of splicing or glycolysis may be able to prevent SARS-CoV–2 replication. Addition of pladeinolide B, a spliceosome inhibitor targeting splicing factor SF3B122, prevented viral replication at conditions non-toxic to the host cells (Fig. 3d, Extended Data Fig. 3c), revealing splicing as an essential pathway for SARS-CoV–2 replication and potential therapeutic target.

Next, we assessed the propensity to inhibit the other main cellular cluster increased upon SARS-CoV–2 infection—carbon metabolism. Indeed, inhibition of glycolysis by 2-deoxy-D-glucose (2-DG), an inhibitor of hexokinase (i.e. glycolysis), had previously been shown to be effective against other viruses in cell culture and suppressed rhinovirus infection in mice23.

Blocking glycolysis with non-toxic concentrations of 2-DG prevented SARS-CoV–2 replication in Caco–2 cells (Fig. 3e and Extended Data Fig. 3d). Together, our quantitative analyses of proteome changes upon SARS-CoV–2 infection revealed host pathways changes upon infection and revealed spliceosome and glycolysis inhibitors as potential

therapeutic agents for COVID–19.

Kinetic proteome profiling to identify potential antiviral targets

In order to better understand host proteins co-increased with viral proteins and to provide with potential additional inhibitors of SARS-CoV–2 replication, we next analysed for proteins showing a similar abundance trajectory over time as viral proteins (Fig. 4a). We computed distance and false discovery rate for each protein compared to the averaged profile of all viral proteins and filtered the data for all proteins with a FDR below 0.01 and performed functional interaction network analysis. Furthermore, in line with our analyses of translatome changes, we found RNA modifying components and metabolic pathways enriched (Extended Data Fig. 3b, c). Next, we carried out gene ontology (GO) analysis of all proteins showing an abundance trajectory significantly similar to the viral protein profile (Supplementary Table 5). We identified a major cluster of metabolic pathways enriched in our data, which consisted of diverse nucleic acid metabolism sub-pathways (Fig. 4b). Coronavirus replication depends on availability of cellular nucleotide pools24,25 Thus, we tested the effect of inhibitors of nucleotide synthesis on SARS-CoV–2 replication in cells. We did not observe any antiviral effects of brequinar, an inhibitor of dihydroorotate dehydrogenase, required for de novo pyrimidine biosynthesis, tested at a maximum concentration of 10 µM. In contrast, ribavirine, which inhibits inosine monophosphate dehydrogenase (IMPDH), the rate-limiting enzyme in *de novo* synthesis of guanosine nucleotides, inhibited SARS-CoV–2 replication at low micromolar concentrations (Fig. 4c and Extended Data Fig. 4a). This is consistent with previous studies showing that targeting IMPDH inhibits replication of coronaviruses HCoV- 43, CoV-NL63 and MERS-CoV16, but strikingly not of SARS-CoV–126. This suggests ribavirine, which is an approved antiviral medication, may be regarded as a possible candidate for further testing. Additionally, components of the protein folding machinery showed a behaviour highly

comparable to the viral proteins (Extended Data Fig. 3e), consistent with a perturbation of host cell proteostasis due to the higher folding load resulting from high translation rates of viral proteins in the cytosol and ER. Therefore, we tested effects of NMS–873, a small molecule inhibitor of the AAA ATPase p97, on SARS-CoV–2 replication. p97 is a key component of proteostasis affecting protein degradation, membrane fusion, vesicular trafficking and disassembly of stress granules27. NMS–873 has been shown to inhibit influenza A and B replication with decreased expression and mislocalization of viral proteins as suggested mechanism28. NMS–873 completely inhibited SARS-CoV–2 at low nanomolar concentrations (Fig. 4d and Extended Data Fig. 4b). In summary, analyses of the effects of SARS-CoV–2 infection on the host cell proteome revealed major readjustments in cellular function, particularly of splicing, proteostasis and nucleotide biosynthesis. Compounds modulating these pathways prevented SARS-CoV–2 replication in cells.

Discussion

Currently, over 80,000 cases of COVID–19 have been reported and the virus continues to spread globally. Therefore, identifying and testing potential drug candidates is of high priority. So far, only very limited data has been obtained describing the cellular response to infection with SARS-CoV–2 preventing the informed assessment of treatment options. We recently communicated the success in isolating SARS-CoV–2 from patients12 and here employed the virus to set up cellular infection assays to allow monitoring the effects of infection on host cells. We used proteomic analyses of the translatome and proteome to allow highly time-resolved insight into the cellular response to SARS-CoV–2 infection and to identify pathways as potential drug targets. Strikingly, the host response was significantly delayed, with extensive antiviral responses, such as shut-down of translation via PKR- dependent activation of the integrated stress response, largely absent (Fig. 2).

For SARS- CoV–1, albeit with overexpression of viral effector proteins instead of infection with wild- type virus, strong effects on translation had been described14,15. This observation suggests that either pseudoviruses or expression of single viral proteins do not faithfully reproduce the host cell effects elicited by an intact, replicative virus, or that SARS-CoV–2 has developed mechanisms to delay or prevent the host cell response. Based on our observations, we tested two translation inhibitors with different modes of action and found these to efficiently prevent viral replication in cells. These findings strongly encourage further testing of translation inhibitors for preventing SARS-CoV–2 replication. Overall, our proteomics analyses suggested cellular pathways for therapeutic intervention, including a profound increase in spliceosome, proteostasis and nucleotide biosynthesis pathway components. Revealing these pathways provided with some drug targets, which were based on the behaviour of SARS-CoV–2 in human cells and had not previously been tested with other coronaviruses. Some of the inhibitors, for which we observed inhibition of SARS- CoV–2, are approved drugs, such ribavirine and emetine, or undergoing clinical trials (i.e. 2- DG).

Our manuscript details a general blueprint for analysis of pathways important for viral infection in cells and to propose likely pathways to inhibit viral replication. Determining possible compounds based on the specific cellular infection profile of the virus allows an unbiased determination of potential drug targets. Here, using such an experimental-data-driven approach, we identified several drugs preventing SARS-CoV–2 replication in cells for further testing in clinical settings for COVID–19.

Declarations

Acknowledgements

We thank Christiane Pallas and Lena Stegmann for support of with the experimental work

and Georg Tascher and Martin Adrian-Allgood for mass spectrometry support. J. C. acknowledges funding by the Hilfe für krebskranke Kinder Frankfurt e.V. and the Frankfurter Stiftung für krebskranke Kinder. C. M. was supported by the European Research Council under the European Union's Seventh Framework Programme (ERC StG 803565), the Emmy Noether Programme of the Deutsche Forschungsgemeinschaft (DFG, MU 4216/1–1), the Johanna Quandt Young Academy at Goethe, and Aventis Foundation Bridge Award.

Contributions

B. K., J. C. and C. M. conceived the study. D. M., carried out tissue culture work, virus experiments, and cytotoxicity assays. K. K. performed proteomic analyses of viral infection kinetics and bioinformatics analyses. M. W. carried out quantitative PCRs. B. K. analysed literature for established inhibitors in viral therapy. D. K. developed the online tool for data visualization. S. C., J. C. and C. M. supervised the work. K. K., J. C. and C. M. wrote the initial manuscript, with contributions from all authors. All authors read and approved the final manuscript.

Competing interests

The authors declare no competing interests.

Materials & correspondence

Correspondence and material requests to Jindrich Cinatl or Christian Münch.

References

1. Zhu, N. *et al.* A Novel Coronavirus from Patients with Pneumonia in China, 2019. *Engl. J. Med.* **382**, 727–733 (2020).
2. Dong, E., Du, H. & Gardner, L. An interactive web-based dashboard to track COVID-19 in real time. *Lancet Infect. Dis.* (2020).

3. Huang, C. *et al.* Clinical features of patients infected with 2019 novel coronavirus in Wuhan, China. *Lancet* (2020).
4. Wang, D. *et al.* Clinical characteristics of 138 hospitalized patients with 2019 novel coronavirus–infected pneumonia in Wuhan, China. *Jama* (2020).
5. Chen, N. *et al.* Epidemiological and clinical characteristics of 99 cases of 2019 novel coronavirus pneumonia in Wuhan, China: a descriptive study. *Lancet* (2020).
6. Chan, J. F.-W. *et al.* A familial cluster of pneumonia associated with the 2019 novel coronavirus indicating person-to-person transmission: a study of a family cluster. *Lancet* (2020).
7. Zhao, S. *et al.* Preliminary estimation of the basic reproduction number of novel coronavirus (2019-nCoV) in China, from 2019 to 2020: A data-driven analysis in the early phase of the outbreak. *J. Infect. Dis.* (2020).
8. Tang, B. *et al.* Estimation of the Transmission Risk of the 2019-nCoV and Its Implication for Public Health Interventions. *Clin. Med.* **9**, 462 (2020).
9. She, J. *et al.* 2019 novel coronavirus of pneumonia in Wuhan, China: emerging attack and management strategies. *Transl. Med.* **9**, 1–7 (2020).
10. Jin, Y.-H. *et al.* A rapid advice guideline for the diagnosis and treatment of 2019 novel coronavirus (2019-nCoV) infected pneumonia (standard version). *Med. Res.* **7**, 4 (2020).
11. Pillaiyar, T., Meenakshisundaram, S. & Manickam, M. Recent discovery and development of inhibitors targeting coronaviruses. *Drug Discov. Today* (2020).
12. Hoehl, S. *et al.* Evidence of SARS-CoV-2 Infection in Returning Travelers from Wuhan, China. *Engl. J. Med.* (2020).
13. Klann, K., Tascher, G. & Münch, C. Functional Translatome Proteomics Reveal Converging and Dose-Dependent Regulation by mTORC1 and eIF2α. *Cell* **77**, 913-

925.e4 (2020).

14. Stern-Ginossar, N., Thompson, S. R., Mathews, M. B. & Mohr, I. Translational Control in Virus-Infected Cells. *Cold Spring Harb. Perspect. Biol.* **11**, (2019).

15. Mohr, I. & Sonenberg, N. Host Translation at the Nexus of Infection and Immunity *Cell Host Microbe* **12**, 470–483 (2012).

16. Shen, *et al.* High-throughput screening and identification of potent broad-spectrum inhibitors of coronaviruses. *J. Virol.* **93**, e00023-19 (2019).

17. Jourdan, S. S., Osorio, F. & Hiscox, J. A. An interactome map of the nucleocapsid protein from a highly pathogenic N orth A merican porcine reproductive and respiratory syndrome virus strain generated using SILAC-based quantitative proteomics. *Proteomics* **12**, 1015–1023 (2012).

18. Emmott, E. *et al.* The cellular interactome of the coronavirus infectious bronchitis virus nucleocapsid protein and functional implications for virus biology. *Virol.* **87**, 9486– 9500 (2013).

19. Neuman, B. W. *et al.* Proteomics analysis unravels the functional repertoire of coronavirus nonstructural protein 3. *Virol.* **82**, 5279–5294 (2008).

20. Wong, H. H. *et al.* Genome-wide screen reveals valosin-containing protein requirement for coronavirus exit from endosomes. *Virol.* **89**, 11116–11128 (2015).

21. Song, T. *et al.* Quantitative interactome reveals that porcine reproductive and respiratory syndrome virus nonstructural protein 2 forms a complex with viral nucleocapsid protein and cellular vimentin. *Proteomics* **142**, 70–81 (2016).

22. Cretu, C. *et al.* Structural Basis of Splicing Modulation by Antitumor Macrolide Compounds. *Cell* **70**, 265-273.e8 (2018).

23. Gualdoni, G. A. *et al.* Rhinovirus induces an anabolic reprogramming in host cell metabolism essential for viral replication. *Natl. Acad. Sci.* **115**, E7158 LP-E7165

(2018).

24. Saijo, M. *et al.* Inhibitory effect of mizoribine and ribavirin on the replication of severe acute respiratory syndrome (SARS)-associated coronavirus. *Antiviral Res.* **66**, 159–163 (2005).

25. Pruijssers, A. J. & Denison, M. R. Nucleoside analogues for the treatment of coronavirus infections. *Opin. Virol.* **35**, 57–62 (2019).

26. Cinatl, J. *et al.* Glycyrrhizin, an active component of liquorice roots, and replication of SARS-associated coronavirus. *Lancet* **361**, 2045–2046 (2003).

27. Ye, Y., Tang, W. K., Zhang, T. & Xia, D. A Mighty “Protein Extractor” of the Cell: Structure and Function of the p97/CDC48 ATPase . *Frontiers in Molecular Biosciences* **4**, 39 (2017).

28. Zhang, J. *et al.* Identification of NMS-873, an allosteric and specific p97 inhibitor, as a broad antiviral against both influenza A and B viruses. *J. Pharm. Sci.* **133**, 86–94 (2019).

29. Corman, V. M. *et al.* Detection of 2019 novel coronavirus (2019-nCoV) by real-time RT-PCR. *Euro Surveill.* **25**, 2000045 (2020).

30. Plubell, D. *et al.* Extended Multiplexing of Tandem Mass Tags (TMT) Labeling Reveals Age and High Fat Diet Specific Proteome Changes in Mouse Epididymal Adipose Tissue. *Mol. Cell. Proteomics* **16**, 873–890 (2017).

31. Robinson, M. D. & Oshlack, A. A scaling normalization method for differential expression analysis of RNA-seq data. *Genome Biol.* **11**, R25 (2010).

32. McKinney, W. Data Structures for Statistical Computing in Python. 51–56 (2010).

33. van der Walt, S., Colbert, S. C. & Varoquaux, G. The NumPy Array: A Structure for Efficient Numerical Computation. *Sci. Eng.* **13**, 22–30 (2011).

34. Tyanova, S. *et al.* The Perseus computational platform for comprehensive analysis of

(prote)omics data. *Methods* **13**, 731–740 (2016).

35. Shannon, P. *et al.* Cytoscape: a software environment for integrated models of biomolecular interaction networks. *Genome Res.* **13**, 2498–504 (2003).

36. Maere, S., Heymans, K. & Kuiper, M. BiNGO: a Cytoscape plugin to assess overrepresentation of Gene Ontology categories in Biological Networks. *Bioinformatics* **21**, 3448–3449 (2005).

37. Merico, D., Isserlin, R., Stueker, O., Emili, A. & Bader, G. D. Enrichment Map: A Network-Based Method for Gene-Set Enrichment Visualization and Interpretation. *PLoS One* **5**, e13984 (2010).

38. Wu, G. & Haw, R. Functional Interaction Network Construction and Analysis for Disease Discovery. in 235–253 (Humana Press, New York, NY, 2017). doi:10.1007/978-1-4939-6783-4_11

39. Perez-Riverol, Y. *et al.* The PRIDE database and related tools and resources in 2019: improving support for quantification data. *Nucleic Acids Res.* **47**, D442–D450 (2019).

Methods

Cell culture

Human Caco–2 cells, derived from colon carcinoma, was obtained from the Deutsche Sammlung von Mikroorganismen und Zellkulturen (DSMZ; Braunschweig, Germany). Cells were grown at 37°C in Minimal Essential Medium (MEM) supplemented with 10% fetal bovine serum (FBS) and containing 100 IU/ml penicillin and 100 µg/ml streptomycin. All culture reagents were purchased from Sigma.

Virus preparation

SARS-CoV–2 was isolated from samples of travellers returning from Wuhan (China) to Frankfurt (Germany) using human colon carcinoma cell line CaCo–2 as described

previously12. SARS-CoV–2 stocks used in the experiments had undergone one passage on CaCo–2 cells and were stored at –80° C. Virus titers were determined as TCID50/ml in confluent cells in 96-well microtiter plates.

Quantification of viral RNA

SARS-CoV–2 RNA from cell culture supernatant samples was isolated using AVL buffer and the QIAamp Viral RNA Kit (Qiagen) according to the manufacturer's instructions. Absorbance-based quantification of the RNA yield was performed using the Genesys 10S UV-Vis Spectrophotometer (Thermo Scientific). RNA was subjected to OneStep qRT-PCR analysis using the Luna Universal One-Step RT-qPCR Kit (New England Biolabs) and a CFX96 Real-Time System, C1000 Touch Thermal Cycler. Primers were adapted from the WHO protocol29 targeting the open reading frame for RNA-dependent RNA polymerase (RdRp): RdRP_SARSr-F2 (GTG ARA TGG TCA TGT GTG GCG G) and RdRP_SARSr-R1 (CAR ATG TTA AAS ACA CTA TTA GCA TA) using 0.4 µM per reaction. Standard curves were created using plasmid DNA (pEX-A128-RdRP) harboring the corresponding amplicon regions for RdRP target sequence according to GenBank Accession number NC_045512. For each condition three biological replicates were used. Mean and standard deviation were calculated for each group.

Antiviral and cell viability assays

Confluent layers of CaCo–2 cells in 96-well plates were infected with SARS-CoV–2 at MOI 0.01. Virus was added together with drugs and incubated in MEM supplemented with 2% FBS with different drug dilutions. Cytopathogenic effect (CPE) was assessed visually 48 h after infection. To assess effects of drugs on Caco–2 cell viability, confluent cell layers were treated with different drug concentration in 96-well plates. The viability was measured using the Rotitest Vital (Roth) according to manufacturer's instructions. Data for

each condition was collected for at least three biological replicates. For dose response curves, data was fitted with all replicates using OriginPro 2020 with the following equation:

$$y = A1 + \frac{A2 - A1}{1 + 10^{(LOGx0 - x)p}}$$

IC50 values were generated by Origin together with metrics for curve fits.

Isotope labelling and cell lysis

Two hours before harvest cells were washed twice with warm PBS to remove interfering medium and cultured for two additional hours with DMEM medium containing 84 mg/L L-Arginine (13C615N4; Cambridge Isotope Laboratories, Cat#CNLM–539-H) and 146 mg/L L-Lysine (13C615N2, Cambridge Isotope Laboratories, Cat#CNLM–291-H) to label nascent proteins. After labelling, the cells were washed three times with room temperature PBS and lysed with 95° C hot lysis buffer (100mM EPPS pH 8.2, 2% sodium deoxycholate, 1mM TCEP, 4 mM 2-Chloracetamide, Protease inhibitor tablet mini EDTA-free [Roche]). Samples were then incubated for additional five minutes at 95° C, followed by sonication for 30 s and further 10 min incubation at 95° C.

Sample preparation for mass spectrometry

Samples were prepared as previously described13. Briefly, proteins were precipitated using methanol/chloroform precipitation and resuspended in 8 M Urea/10 mM EPPS pH 8.2. Isolated proteins were digested with 1:50 wt/wt LysC (Wako Chemicals) and 1:100 wt/wt Trypsin (Promega, Sequencing grade) overnight at 37°C after dilution to a final Urea concentration of 1 M. Then, digests were acidified (to pH 2–3) using TFA. Peptides were purified using C18 (50 mg) SepPak columns (Waters) as previously described. Desalted

peptides were dried and 25 µg of peptides were resuspended in TMT labelling buffer (200 mM EPPS pH 8.2, 10% acetonitrile). Peptides were subjected to TMT labelling with 1:2 Peptide TMT ratio (wt/wt) for one hour at room temperature. Labelling reaction was quenched by addition of hydroxylamine to a final concentration of 0.5% and incubation at room temperature for additional 15 min. Labelled peptides were pooled and subjected to High pH Reverse Phase fractionation with the HpH RP Fractionation kit (Thermo Fisher Scientific) following manufacturer's instructions. All multiplexes were mixed with a bridge channel, that consists of control sample labelled in one reaction and split to all multiplexes in equimolar amounts.

Liquid chromatography mass spectrometry

Peptides were resuspended in 0.1% FA and separated on an Easy nLC 1200 (ThermoFisher Scientific) and a 22 cm long, 75 µm ID fused-silica column, which had been packed in house with 1.9 µm C18 particles (ReproSil-Pur, Dr. Maisch), and kept at 45°C using an integrated column oven (Sonation). Peptides were eluted by a non-linear gradient from 5–38% acetonitrile over 120 min and directly sprayed into a QExactive HF mass spectrometer equipped with a nanoFlex ion source (ThermoFisher Scientific) at a spray voltage of 2.3 kV. Full scan MS spectra (350–1400 m/z) were acquired at a resolution of 120,000 at m/z 200, a maximum injection time of 100 ms and an AGC target value of 3 x 106. Up to 20 most intense peptides per full scan were isolated using a 1 Th window and fragmented using higher energy collisional dissociation (normalized collision energy of 35). MS/MS spectra were acquired with a resolution of 45,000 at m/z 200, a maximum injection time of 80 ms and an AGC target value of 1 x 105. Ions with charge states of 1 and > 6 as well as ions with unassigned charge states were not considered for fragmentation. Dynamic exclusion was set to 20 s to minimize repeated sequencing of already acquired precursors.

Mass spectrometry data analysis

Raw files were analysed using Proteome Discoverer (PD) 2.4 software (ThermoFisher Scientific). Spectra were selected using default settings and database searches performed using SequestHT node in PD. Database searches were performed against trypsin digested Homo Sapiens SwissProt database, SARS-CoV–2 database (Uniprot pre-release) and FASTA files of common contaminants (‘contaminants.fasta’ provided with MaxQuant) for quality control. Fixed modifications were set as TMT6 at the N-terminus and carbamidomethyl at cysteine residues. One search node was set up to search with TMT6 (K) and methionine oxidation as static modifications to search for light peptides and one search node was set up with TMT6+K8 (K, +237.177), Arg10 (R, +10.008) and methionine oxidation as static modifications to identify heavy peptides. Searches were performed using Sequest HT. After search, posterior error probabilities were calculated and PSMs filtered using Percolator using default settings. Consensus Workflow for reporter ion quantification was performed with default settings, except the minimal signal-to-noise ratio was set to 5. Results were then exported to Excel files for further processing. For proteome quantification all PSMs were summed intensity normalized, followed by IRS30 and TMM31 normalization and peptides corresponding to a given UniProt Accession were summed including all modification states.

For translatome measurements excel files were used as input for a custom made in-house Python pipeline. Python 3.6 was used together with the following packages: pandas 0.23.432, numpy 1.15.433, scipy 1.3.0. Excel files with normalized PSM data were read in and each channel was normalized to the lowest channel based on total intensity. For each peptide sequence, all possible modification states containing a heavy label were extracted and the intensities for each channel were averaged between all modified peptides. Baseline subtraction was performed by subtracting the measured intensities for the non-

SILAC- labelled sample from all other values. Negative intensities were treated as zero. The heavy label incorporation at the protein level was calculated by summing the intensities of all peptide sequences belonging to one unique protein accession. These values were combined with the standard protein output of PD 2.4 to add annotation data to the master protein accessions.

Hierarchical clustering and profile comparison

Hierarchical cluster analysis and comparison with viral protein profiles for all samples was performed using Perseus34 software package (version 1.6.5.0) after centering and scaling of data (Z scores). K-means pre-processing was performed with a cluster number of 12 and a maximum of 10 iterations. For the comparison of profiles, the viral profiles were Z scored and averaged to generate reference profile. Profiles of all proteins were compared to the reference (Pearson), distances and False discovery rates computed.

Network analysis

For network analysis, Cytoscape 3.7.1 35 software was used with BiNGO 3.0.3 36 plugin for GO term analysis, EnrichmentMap 3.1.0 37 and ReactomeFI 6.1.0 38. For GO-term analyses, gene sets were extracted from data as indicated using significance cutoffs (P value < 0.05).

Statistical analysis

Significance was, unless stated otherwise, tested using unpaired two-sided students t-tests with equal variance assumed. Statistical analysis was performed using OriginPro 2020 analysis software. For network and GO analysis all statistical computations were performed by the corresponding packages.

Data availability

The mass spectrometry proteomics data have been deposited to the ProteomeXchange

Consortium via the PRIDE39 partner repository with the dataset identifier PXD017710. We furthermore created a webpage (*http://corona.papers.biochem2.com/)* visualizing the presented data for easy access of the published data.

Supplemental Table Information

Table S1 | Data of translatome measurements by MS. Contains Uniprot Accession, Species annotation, Gene Symbol and normalized translation data for each replicate. Log2 ratios and P values were computed for each group comparison. See Fig. 2.

Table S2 | Data of proteome measurements by MS. Contains UniProt Accession, Gene Symbol and normalized protein abundances for each sample. Log2 ratios and P values were computed for each group comparison. See Fig. 3, 4.

Table S3 | Results of Reactome pathway analysis of genes decreased in protein level during infection (Fig. 3a, S3). Pathway names, size of pathway, proteins found in dataset, P values and FDR are given.

Table S4 | Results of Reactome pathway analysis of genes increased in protein level during infection (Fig. 3a, b). Pathway names, size of pathway, proteins found in dataset, P values and FDR are given.

Table S5 |Results of gene ontology (biological process) analysis of genes following viral gene expression (Fig. 4). GO term, proteins found in dataset, GO size, P value and FDR are given.

Figures

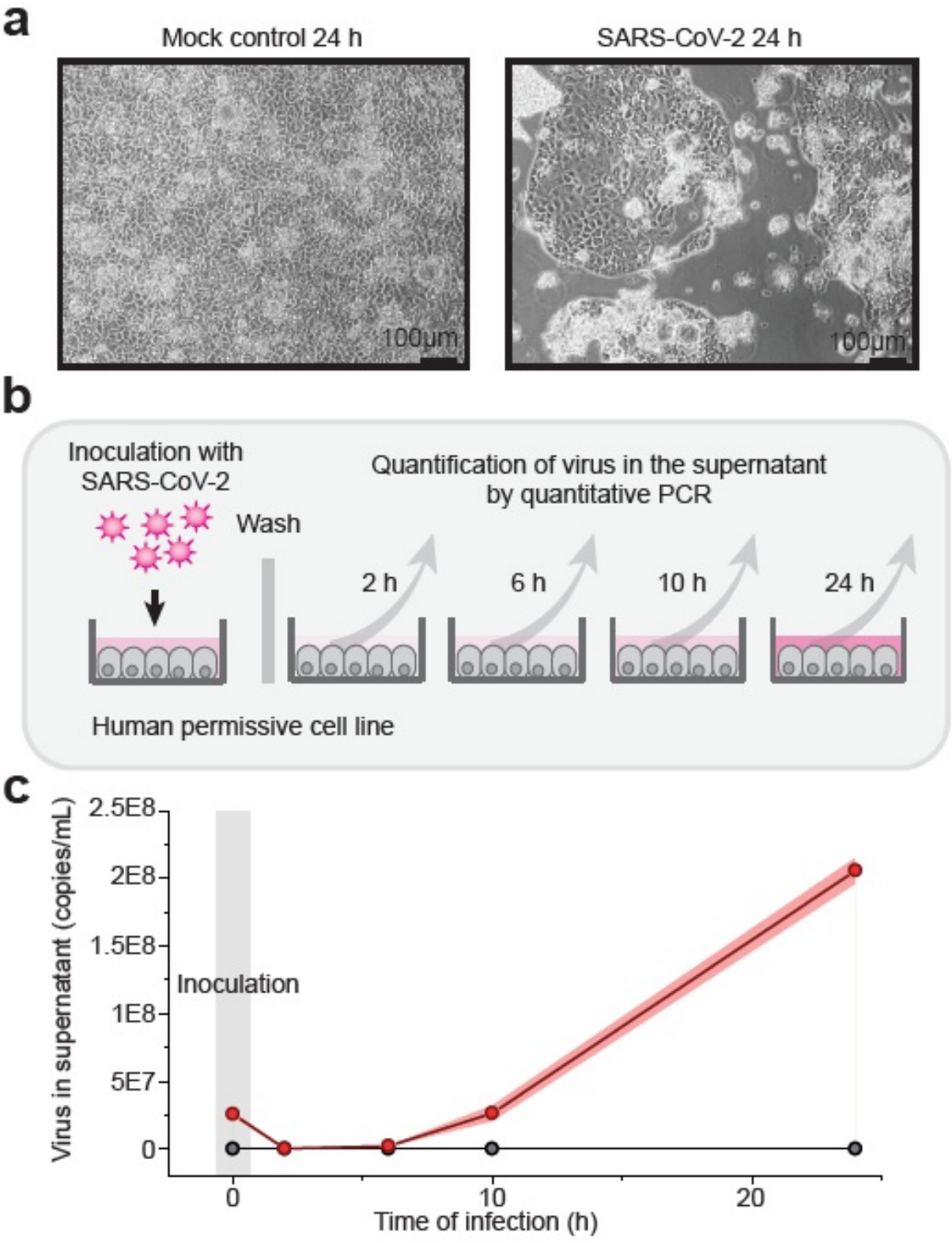

Figure 1

SARS-CoV-2 replicates rapidly in cell line model. a, Caco-2 cells were either mock

or SARS-CoV-2 infected and cultured for 24 h. Microscopy pictures were taken to demonstrate CPE. Scale bars indicate 100 µm. b, Scheme represen□ng experimental design for quantitative virus profiling in cell culture supernatant. Cells were either mock or SARS-CoV-2 infected with an MOI of 1. The inocula□on sample was taken at the first time point as control. Samples from supernatant were obtained in triplicate after 2, 6, 10 and 24 hours and profiled for virus genome by qPCR. c, quantitative PCR analysis of viral genome copies per mL cell culture after indicated infection time points (n = 3). Points indicate mean of replicate measurements and shades represent SD.

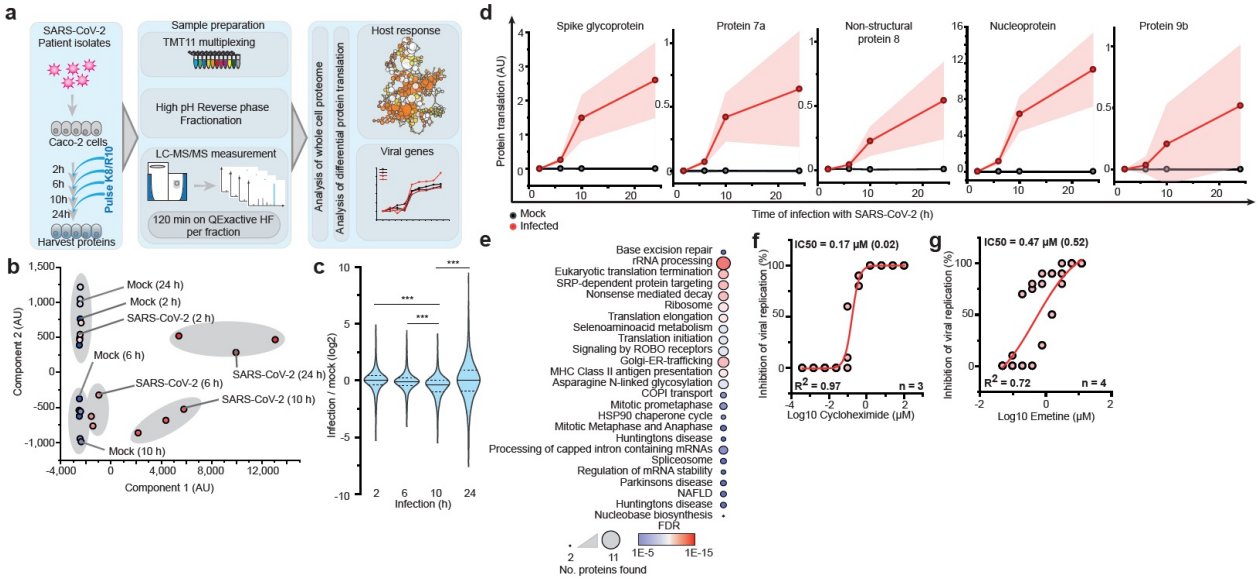

Figure 2

SARS-CoV-2 virus replication is translation sensitive. a, Experimental scheme for translatome and proteome measurements. Caco-2 cells were infected with SARS-CoV-2 isolated from patients and incubated for indicated times. Two hours before harvest, medium was exchanged to heavy SILAC medium to label nascent proteins. Samples were TMT11 labelled for multiplexing, fractionated and measured by LC-MS/MS. Proteome and translatome analysis was carried out to characterize host response and viral gene expression. b, Principal component

analysis of translatome measurements. All samples were filtered for missing values before PCA analysis. c, Global translation rates, showed by distribution plots of fold changes (log2) to mock control for each time point. Significance was tested by one way ANOVA and two sided post-hoc Bonferroni test. *** P value <0.001; n = 3 biological replicates. d, Translation of viral proteins over time. Mean translation is plotted for control and infected samples. Shades indicate SD, n = 3 biological replicates. e, Reactome pathway analysis of top 10% proteins following viral gene expression. Pathway results are shown with number of proteins found in dataset and computed FDR for pathway enrichment. f, g, Antiviral assay showing inhibition of viral replication in dependency of cycloheximide (f, n = 3) and emetine (g, n = 4) concentration. Each data point indicates biological replicates and red line shows dose response curve fit. R2 and IC50 values were computed from the curve fit and SD of IC50 is indicated in brackets. See also Table S1.

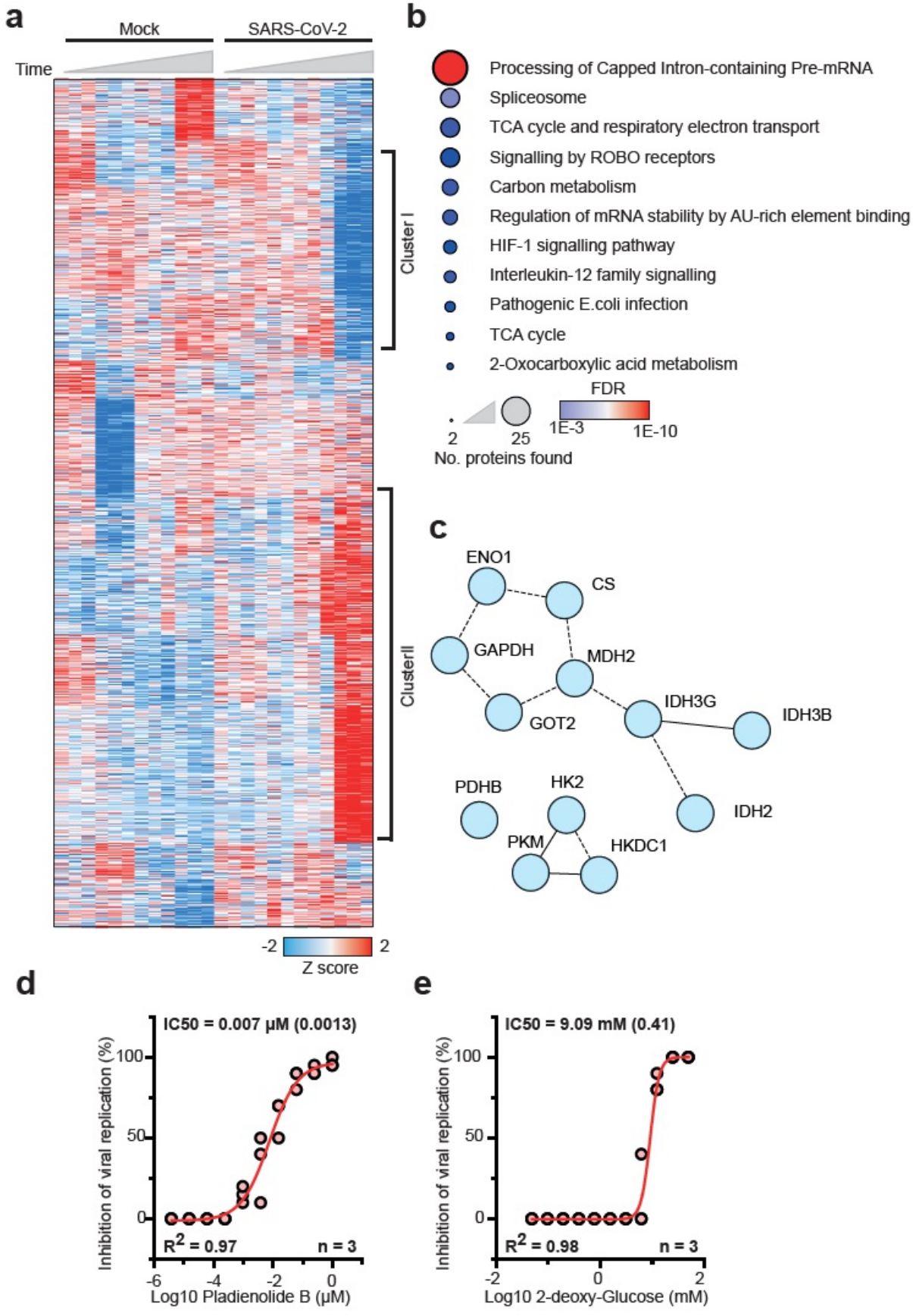
a
Mock
SARS-CoV-2
Time
Cluster I
ClusterII
-2
2
Z score
b
Processing of Capped Intron-containing Pre-mRNA
Spliceosome
TCA cycle and respiratory electron transport
Signalling by ROBO receptors
Carbon metabolism
Regulation of mRNA stability by AU-rich element binding
HIF-1 signalling pathway
Interleukin-12 family signalling
Pathogenic E.coli infection
TCA cycle
2-Oxocarboxylic acid metabolism
FDR
1E-3
1E-10
2
25
No. proteins found
c
ENO1
CS
GAPDH
MDH2
GOT2
IDH3G
IDH3B
PDHB
HK2
IDH2
PKM
HKDC1
d
IC50 = 0.007 μM (0.0013)
Inhibition of viral replication (%)
100
50
0
R2 = 0.97
n = 3
-6
-4
-2
0
Log10 Pladienolide B (μM)
e
IC50 = 9.09 mM (0.41)
Inhibition of viral replication (%)
100
50
0
R2 = 0.98
n = 3
-2
0
2
Log10 2-deoxy-Glucose (mM)

Figure 3

Reprogrammed metabolic pathways indicate treatment sensitivity. a, Patterns of protein levels over all samples. Shown are proteins tested significant (two-sided unpaired t-test with equal variance assumed, $P < 0.05$) in at least one infected sample compared to corresponding control. Data was standardized using Z scoring before row-wise clustering and plotting. b, Reactome pathway analysis of protein network created from cluster II (a, see Table S4). Pathway results are shown with number of proteins found in dataset and computed FDR for pathway enrichment. c, Functional interaction network of proteins found annotated to carbon metabolism in Reactome pathway analysis. Lines indicate functional interaction. d, e, Antiviral assay showing inhibition of viral replication in dependency of pladienolide B (d, $n = 3$) and 2-deoxy-glucose (e, $n = 4$) concentration. Each data point indicates a biological replicate and red line shows dose response curve fit. R2 and IC50 values were computed from the curve fit and SD of IC50 is indicated in brackets. See also Tables S2, S3, S4.

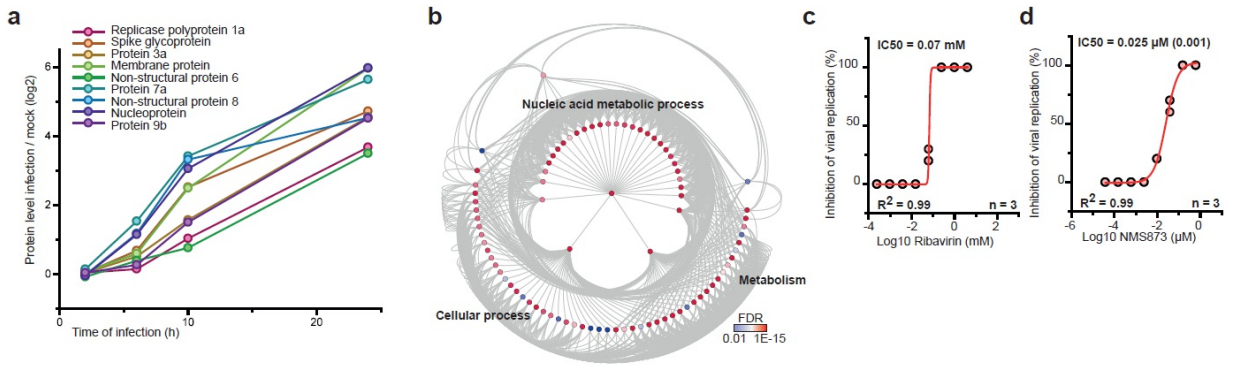

Figure 4

Protein levels of nucleic acid metabolism genes correlate with viral gene expression. a, Protein levels of all detected viral proteins are plotted with their log2 changes to corresponding control for different infection times. Mean fold changes are plotted from three biological replicates. b, Gene ontology network analysis of host proteins correlating with viral protein expression (FDR < 0.01). Proteins were clustered for biological process GO term and plotted as network with FDR colour coding. Annotated pathways represent parent pathways in the network. c, d, Antiviral assay showing inhibition of viral replication in dependency of Ribavirin (c, n = 3) and NMS873 (d, n = 3) concentration. Each data point indicates a biological replicate and red line indicates dose response curve fit. R2 and IC50 values were computed from the curve fit and SD of IC50 is indicated in brackets (for Ribavirin curve fit detected mutual dependency, due to sparse data, no meaningful SD could be computed). See also Table S5.

Supplementary Files

This is a list of supplementary files associated with the primary manuscript. Click to download.

Supplementary Table 03.xlsx
Supplementary Table 04.xlsx
Supplementary Table 05.xlsx

Supplementary Table 01.xlsx
Supplementary Table 02.xlsx
Supplemental figures.pdf